Consiglio Nazionale delle Ricerche
ISTITUTO DI SCIENZE DEL PATRIMONIO CULTURALE

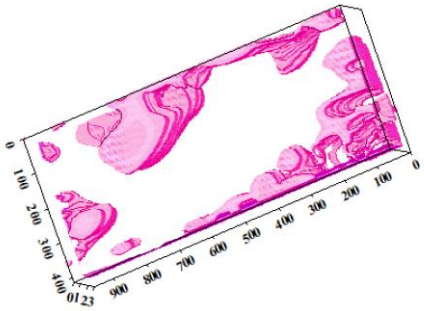

GEOPHYSICAL SURVEY AT ABBATIJA TAD-DEJR HYPOGEUM (RABAT, MALTA)

The Director
Dott.ssa Costanza Miliani

MILIANI
COSTANZA
14.07.2021
12:52:22
UTC

The Scientific Manager
Dott. Giovanni Leucci

Firmato digitalmente
da LEUCCI GIOVANNI
C: IT

JULY 2021

1. ABSTRACT

In order to verify both the presence of hypogean structures and tombs, integrated geophysical surveys, with ground penetrating radar (GPR), and electrical resistivity tomography (ERT), were undertaken at ABBATIJA TAD-DEJR HYPOGEUM (RABAT, MALTA). Furthermore a three-dimensional model of the entire surveyed areas was created.
The integration of the acquired data allows us to plan future excavations.
The surveyed areas are showed in Fig. 1.
The GPR data were collected along grids with parallel profiles set 0.5 m apart, using the Cobra georadar system with the 400MHz and 70MHz antennae. GPR data were processed in 3D using GPR-slice software (Goodman et al. 1994). In order to eliminate a small noise component and make it easy to interpret the GPR data, the following processing sequence was applied:

1) Zero-time adjust (static shift), in order to associate zero-time with zero-depth;
2) Frequency filtering, in order to remove high-frequency noise;
3) Migration, in order to correct the shape and dimension of reflection events related to the structure present in the subsoil.

GPR data were visualized in 3D using both time slice and iso-surface amplitude (Conyers 2012). In this work, the time-slice technique has been used to display the amplitude variations within consecutive time windows of width $\Delta t = 5$ ns. Three-dimensional amplitude iso-surface rendering displays amplitudes of equal value in the GPR data volume. Shading is usually used to illuminate these surfaces, giving the appearance of real archaeological structures. In this case, the threshold calibration is a very delicate task in order to obtain useful results. In order to define the depth of archaeological remains the electromagnetic (EM) wave velocity, using the characteristic hyperbolic shape of a reflection from a point source (diffraction hyperbola), was used (Conyers 2012).
ERT data were collected in a 3D mode along non-conventional profiles (Leucci et al. 2016) using Dipole–Dipole array (Loke 2001) and 1.5m electrode spacing. The ELECTRA, multichannel digital resistivimeter (moho srl) with 32 active channels was used for geoelectrical measurements. The ErtLab inversion software (http://www.geost udias tier.it/) was used for 3D total volume resistivity data distribution in the subsurface.

AREA A: GPR DATA ANALYSIS

In the Area A, 12 GPR profiles were measured. The location of GPR profiles is show in Fig. 2. The results are shows in Figs. 3 and 4. The reflection events labelled “P” are probably related to the pipe line. Other reflection events were generated by the probable presence of buried tombs (“T”). They are located at depth ranging from 0.8m to 1.3m. The reflection event represented by a dashed yellow line (rock) is probably related to the base rock. It is located at depth ranging between 0.4m and 1.0m. With the letter “C” is clearly visible a reflection event at depth ranging from 1.7m and 2.0 m. This event could probabbly related to the presence of cavity. The reflection events labelled “M” are related to metal objects presents at the ground surface (manholes).
The time slices between 0.3m and 2.7m depth are shows in Fig. 5.
In the slice ranging from 0.4 to 0.8 m depth, relatively high-amplitude alignments (dashed dark line) are clearly visible. Particularly evident is the correlation between the reflection event

labelled “P” in 2D radar sections. At depth between 0.9 and 1.0m the high amplitude event “T” is visible. At depth between 1.4 and 2.2m the high amplitude event “C” is visible.

In Fig. 6 the same data set is displayed with iso-amplitude surfaces using a threshold value of 40% of the maximum complex trace amplitude (Leucci 2015). Obviously, lowering the threshold value increases the visibility of the main anomaly and smaller objects, but also of heterogeneous noise. Relatively strong continuous reflections are
visible on the threshold volumes. This visualization technique enhances the visibility of the anomalies related to the archaeological structures (tombs and cavity).

AREA B: GPR DATA ANALYSIS

In the Area B, 16 GPR profiles were measured. The location of GPR profiles is show in Fig. 2. The results are shows in Figs. 7, 8 and 9. The reflection events labelled “P” are probably related to the pipe line. Other reflection events were generated by the probable presence of buried tombs (“T”). They are located at depth ranging from 0.8m to 1.0m. With the letter “M” is clearly visible a shallow reflection event. This event could probabbly related to the presence of metal objects (manholes).

The time slices between 0.3m and 2.0m depth are shows in Figs. 10 and 11.

In the slice ranging from 0.5m to 0.7 m depth (Fig. 10), relatively high-amplitude alignments (dashed dark line) are clearly visible. Particularly evident is the correlation between the reflection event labelled “P” in 2D radar sections.

At depth between 1.3m and 1.8m (Fig. 11) the high amplitude event “T” is visible. At depth between 1.3 and 2.0m (Fig. 11) the high amplitude event “C” is visible.

In Fig. 12 the same data set is displayed with iso-amplitude surfaces using a threshold value of 45% of the maximum complex trace amplitude (Leucci 2015). Relatively strong continuous reflections are visible on the threshold volumes. This visualization technique enhances the visibility of the anomalies related to the archaeological structures (tombs and cavity).

AREA C: GPR DATA ANALYSIS

In the Area C, 15 GPR profiles were measured. The location of GPR profiles is show in Fig. 2. The results are shows in Figs. 13, 14 and 15. The reflection events labelled “P” are probably related to the pipe line. Other reflection events were generated by the probable presence of buried tombs (“T”). They are located at depth ranging from 0.6m to 1.1m. With the letter “M” is clearly visible a shallow reflection event. This event could probabbly related to the presence of metal objects (manholes).

The time slices between 0.0m and 2.5m depth are shows in Fig. 16.

In the slice ranging from 0.0m to 0.3 m depth, relatively high-amplitude alignments are visible. Here evident is the correlation between the reflection event labelled “P” in 2D radar sections.

At depth between 0.5m and 1.3m the high amplitude event “T” is visible. In Fig. 17 the same data set is displayed with iso-amplitude surfaces using a threshold value of 52% of the maximum complex trace amplitude (Leucci 2015). Relatively strong continuous reflections are visible on the threshold volumes. This visualization technique enhances the visibility of the anomalies related to the archaeological structures (tombs).

AREA E: GPR DATA ANALYSIS

In the Area E, 16 GPR profiles were measured. In this case a very low frequency antenna (70MHz) was used. The results are shows as time slices in Fig. 18. Here the time slices between 2.2m and 6.5m depth are show.
In the all showed slices relatively high-amplitude alignments are visible. The high amplitude event located in the upper right corner is related to a visible metal grid. The high amplitude event located in the lower left corner can, probably, related to a cavity.
In Fig. 19 the same data set is displayed with iso-amplitude surfaces using a threshold value of 50% of the maximum complex trace amplitude (Leucci 2015, Leucci, 2019, Leucci, 2020). Relatively strong continuous reflections are visible on the threshold volumes. This visualization technique enhances the visibility of the anomalies related to the archaeological structures (cavity).

AREA D: ERT DATA ANALYSIS

For ERT measurements, in the area D two non-standard profiles were acquired. Initially, a 2D survey is conducted along each perpendicular line or transect. In the next step, the current electrodes remain at the end of one line, while the potential is moved, along the line. Then, the current electrodes move one electrode position and the potential electrodes move as previously described. The process is repeated until the current and potential electrodes cover the L geometry. This sequence of observations produces a series of apparent resistivity observations towards and beneath the central portion of the array. Several L-arrays can be combined to surround a structure to build a 3D matrix of observations (Leucci, 2020). A penetration depth of 6 m was obtained using a total of 64 electrodes deployed within the boundaries of the studied area. After the data acquisition process was performed, the apparent resistivity data were analysed to identify abnormal measurements with a high standard deviation. The investigated volume was computed using the software ErtLab (http://www.geostudiastier.it) that makes use of Finite Elements algorithm.
The depth resistivity slices, that show the resistivity distribution at 0.7 and 2.0 m in depth, are shows in Fig. 20.
At first it is possible to note the presence of a heterogeneous subsurface with resistivity values ranging from 100 to 2000 ohm m. Afterwards, it is possible to note the presence of:

1) areas indicated with ‘‘T’’, with resistivity values between 100 and 150 Ohm m; these values indicate the probable presence of areas where localized tombs. The relatively low resistivity values indicate that these anomalies are not attributable to the presence of empty volumes, but rather to incoherent materials, probably put there in order to fill up the tombs. These areas are at 0.7m depth;

2) areas with resistivity values between 1800 and 2000 ohm m; these values indicate the probable presence of cavity zones.

In Fig. 21 the same data set is displayed with iso-resistivity surfaces using a threshold value of 50% of the maximum resistivity (Leucci, 2020). Relatively strong continuous reflections are visible on the threshold volumes. This visualization technique enhances the visibility of the anomalies related to the archaeological structures (tombs and cavity).

CONCLUSIONS

With the aim of contributing to the advancement in discoveries of the prestigious archaeological site ABBATIJA TAD-DEJR HYPOGEUM, a series of geophysical investigations were undertaken. The visualization in 3D time-slice maps, used mainly to enhance the horizontal relationships between amplitude anomalies found in the standard two dimensional GPR and ERT sections, point to several anomalous zone, interpreted as buried structures of probable tombs and cavity (Figs. 22 and 23).

REFERENCES

Conyers LB (2012) Interpreting ground-penetrating radar for archaeology. Left Coast Press, Walnut Creek

Goodman D, Nishimura Y, Tobita K (1994) GPRSIM forward modeling software and time slices in ground

penetrating radar surveys. In: Proceedings of the fifth international conference on ground penetrating

radar (GPR’94) 12–16 June, Kitchener, Ontario, Canada, pp 31–43

Leucci G, De Giorgi L, Gizzi F, Persico R (2016) Integrated geo-scientific surveys in the historical centre of

Mesagne (Brindisi, Southern Italy). Natural Hazard. https ://doi.org/10.1007/s1106 9-016-2645-x

Leucci G (2015) Geofisica Applicata all’Archeologia e ai Beni Monumentali. Dario Flaccovio Editore, Palermo, p 368

Leucci G., 2019, Nondestructive Testing for Archaeology and Cultural Heritage: A practical guide and new perspective. Springer editore pp 217, ISBN 978-3-030-01898-6

Leucci G., 2020, Advances in Geophysical Methods Applied to Forensic Investigations: New Developments in Acquisition and Data Analysis Methodologies. Springer editore, pp 200, ISBN 978-3-030-46241-3

Loke MH (2001) Electrical imaging surveys for environmental and engineering studies. A practical guide to 2-D and 3-D surveys: RES2DINV manual, IRIS Instruments. http://perso nales .upv.es/jpadi n/coursenote s.pdf

FIGURE

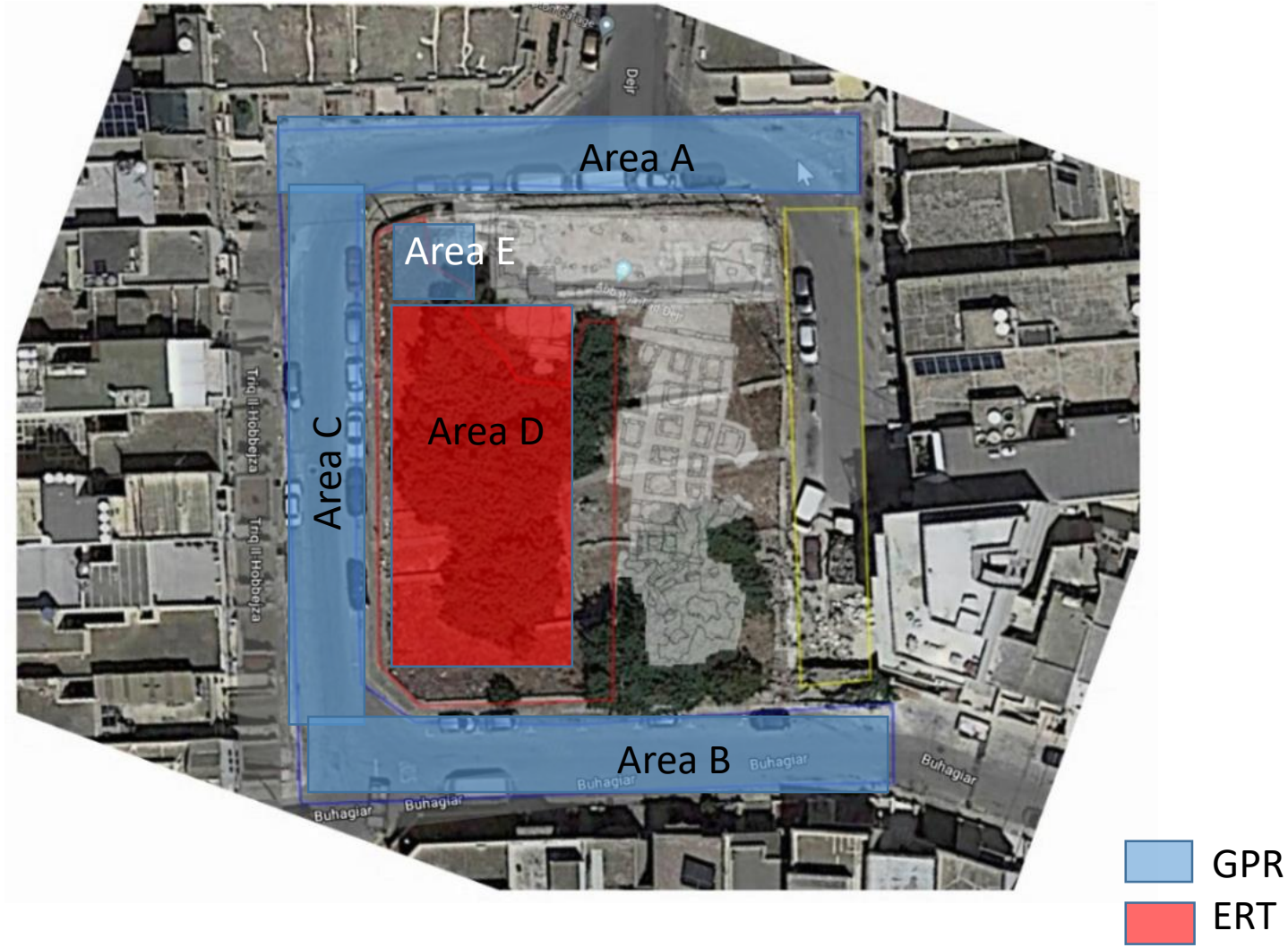

Fig. 1: Surveyed areas

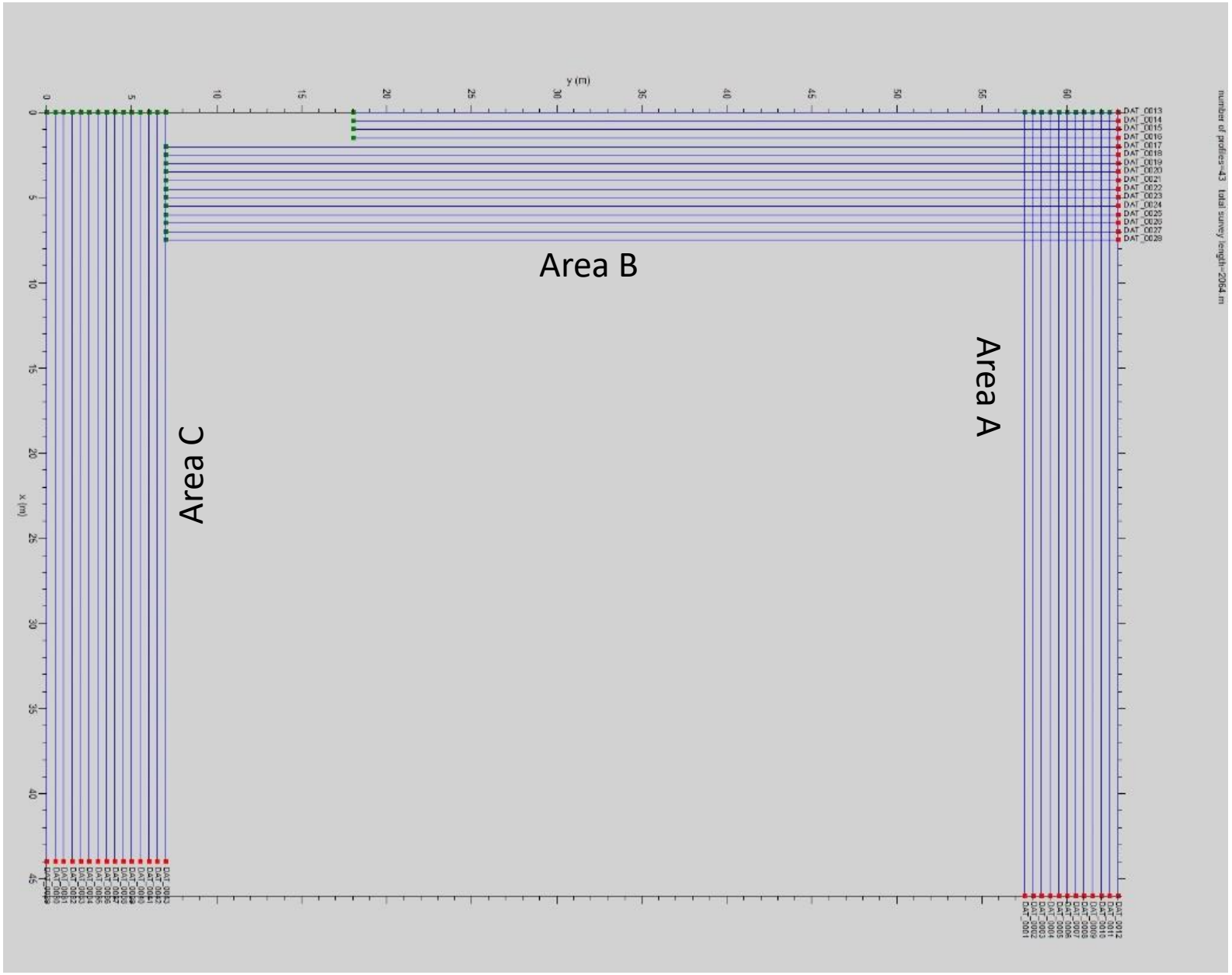

Fig. 2: Location of GPR Profiles

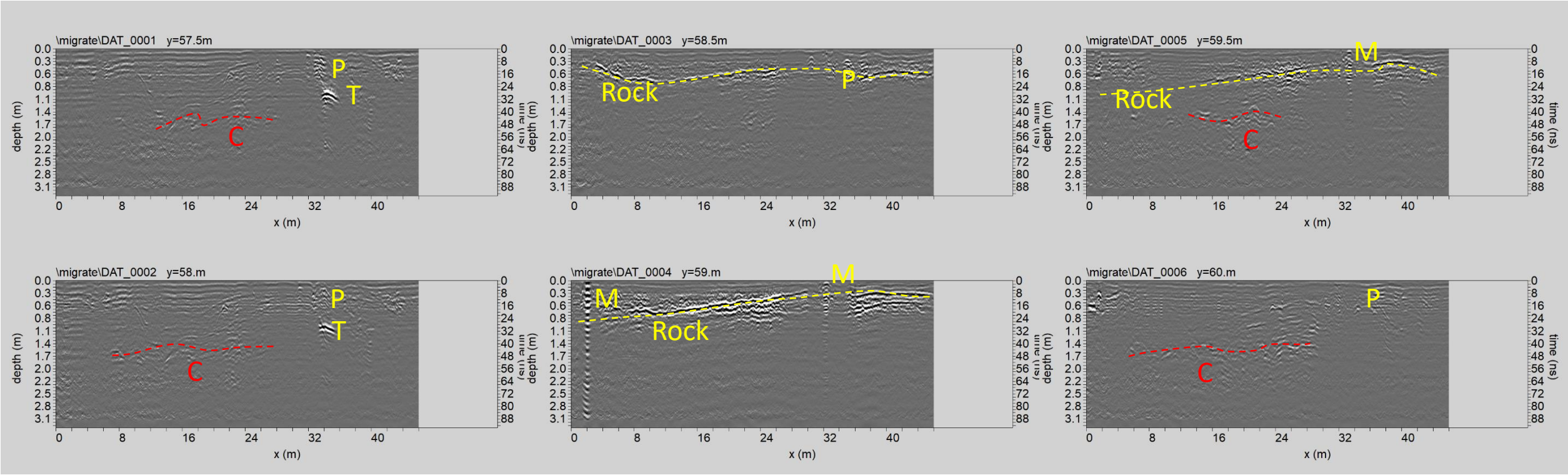

Fig. 3: Area A: GPR data processed related to the profiles 1, …, 6

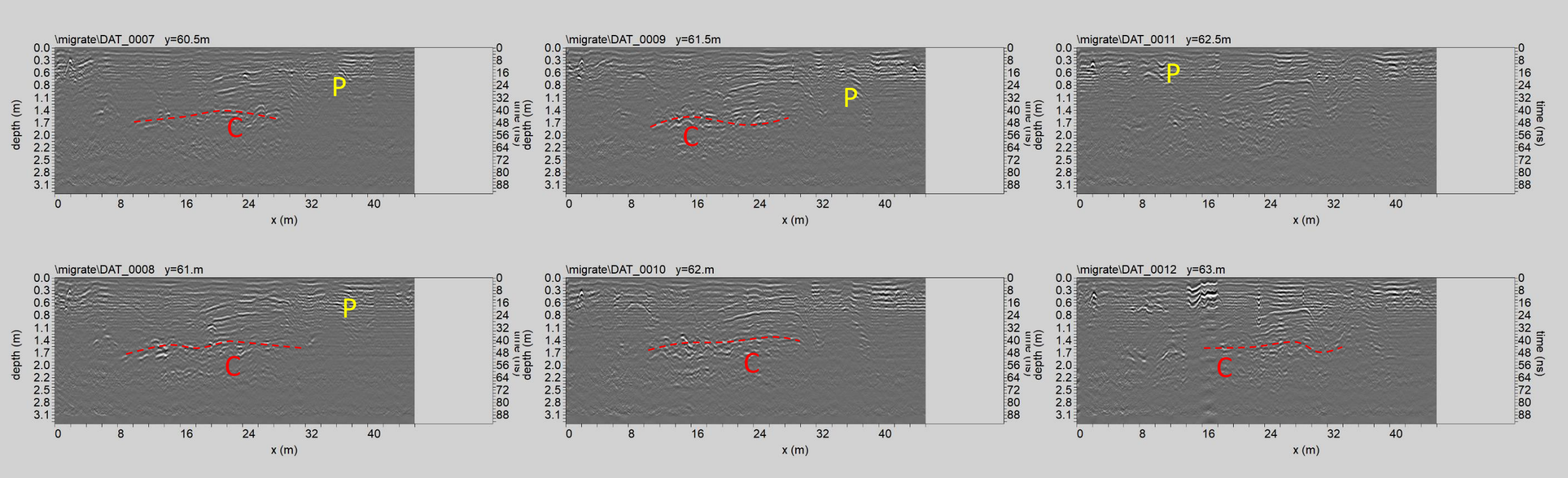

Fig. 4: Area A: GPR data processed related to the profiles 7, …, 12

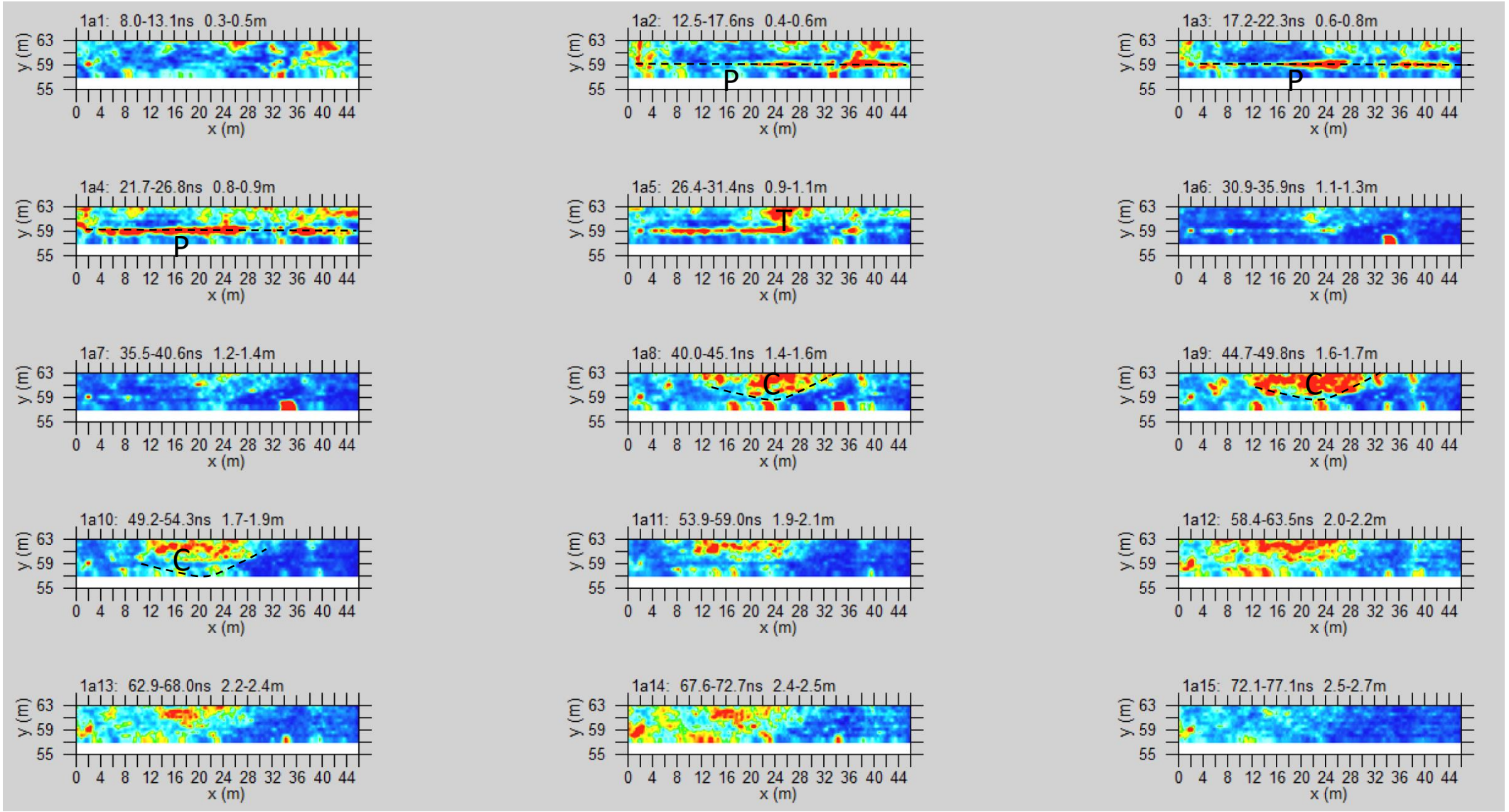

Fig. 5: Area A: Depth slices

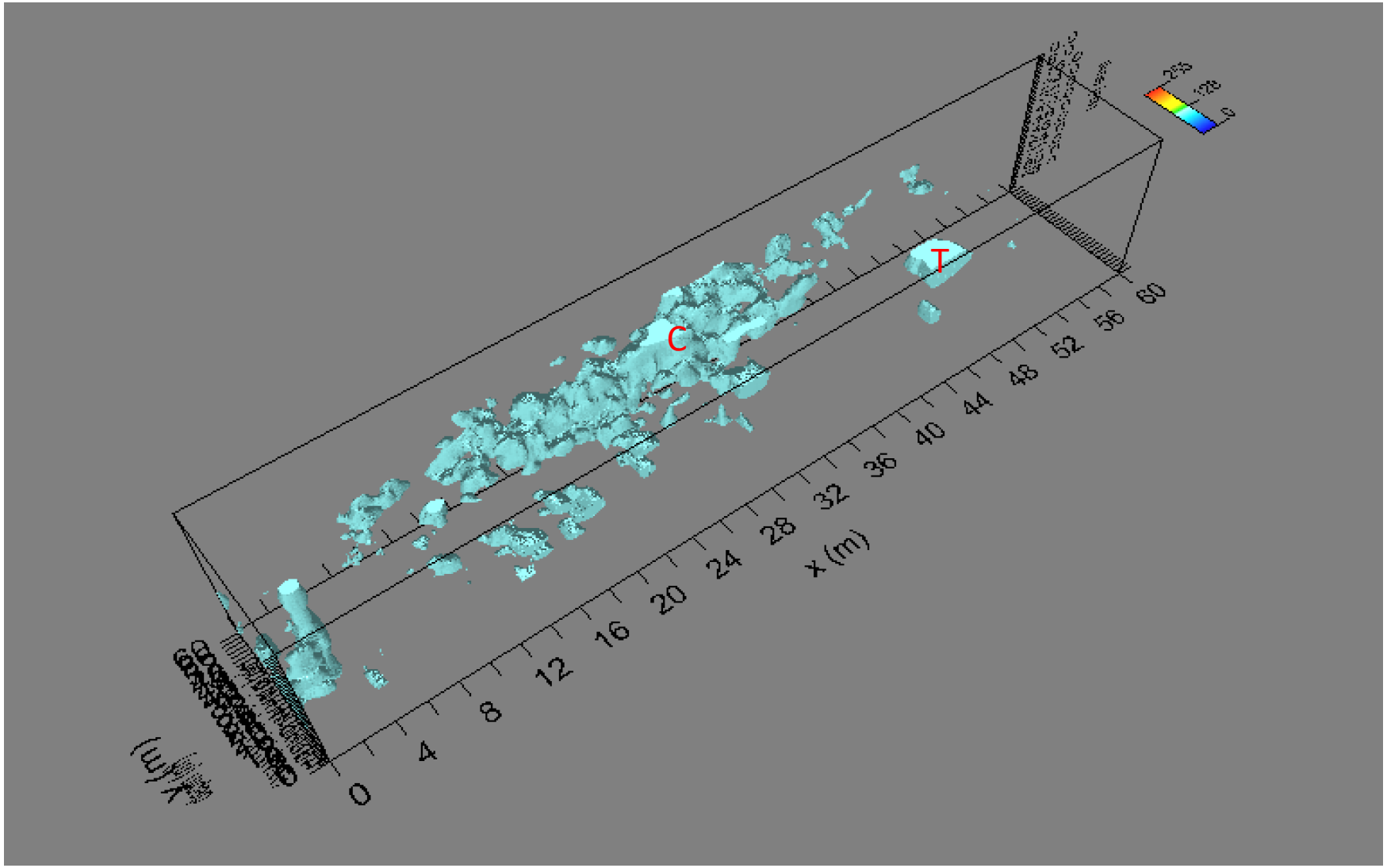

Fig. 6: Area A: iso surfaces

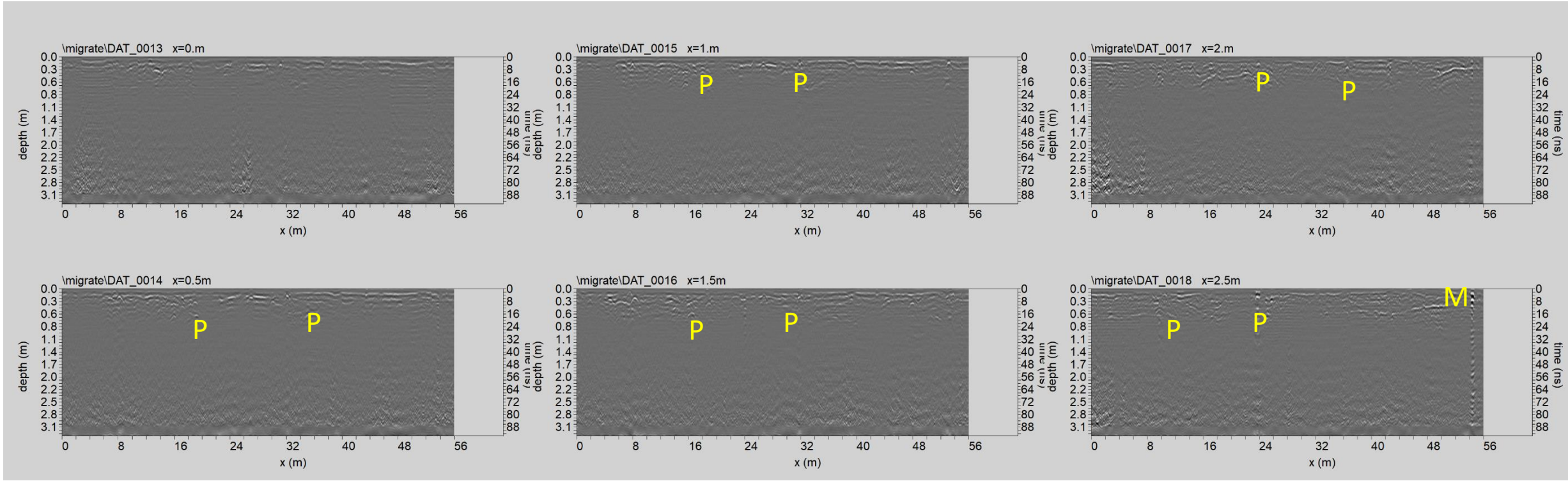

Fig. 7: Area B: GPR data processed related to the profiles 13, …, 18

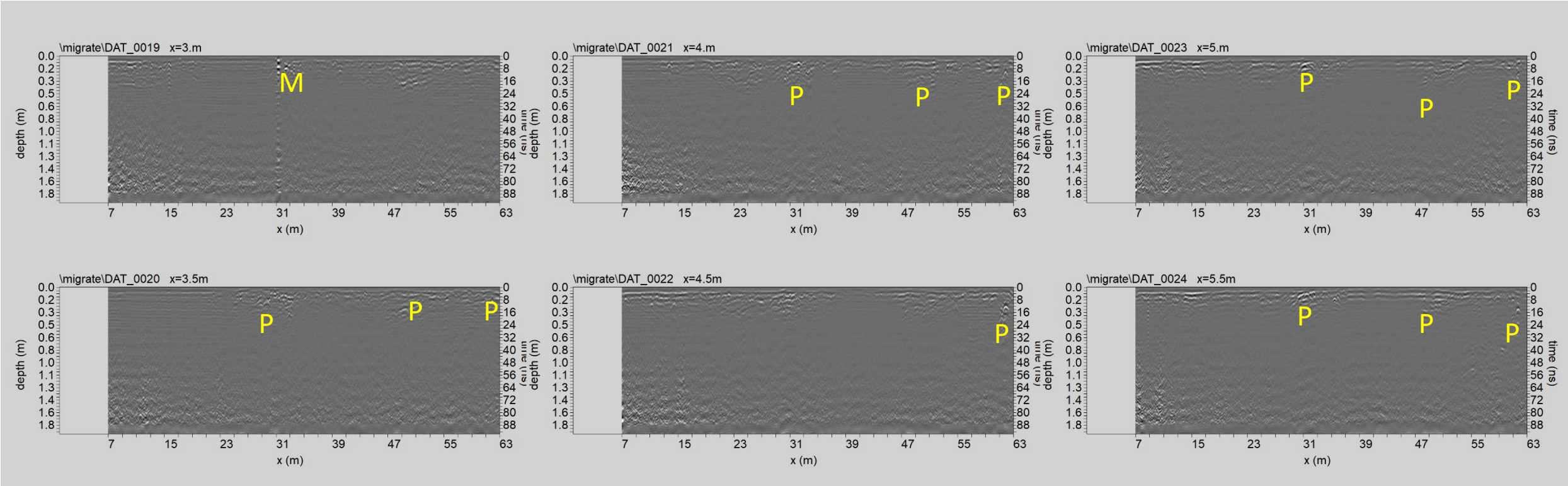

Fig. 8: Area B: GPR data processed related to the profiles 19, …, 24

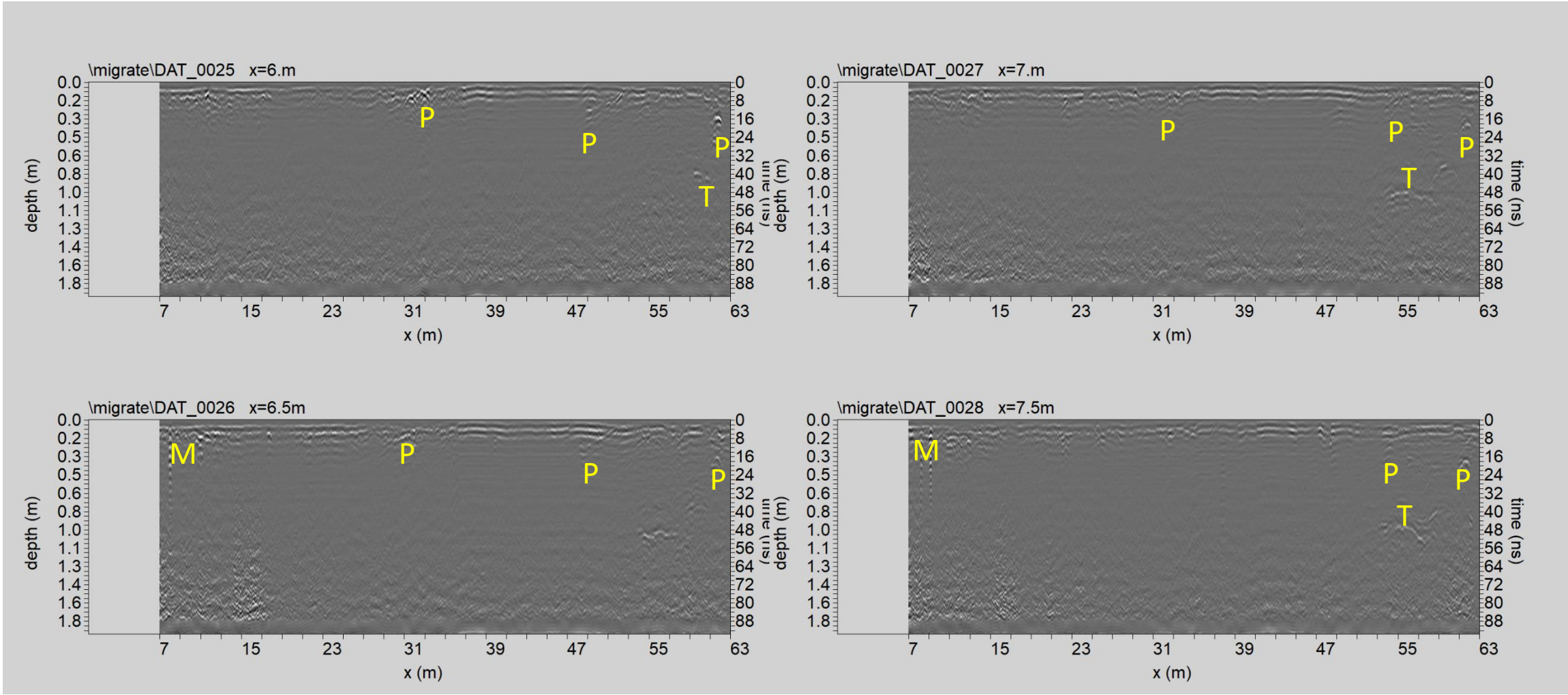

Fig. 9: Area B: GPR data processed related to the profiles 25, …, 28

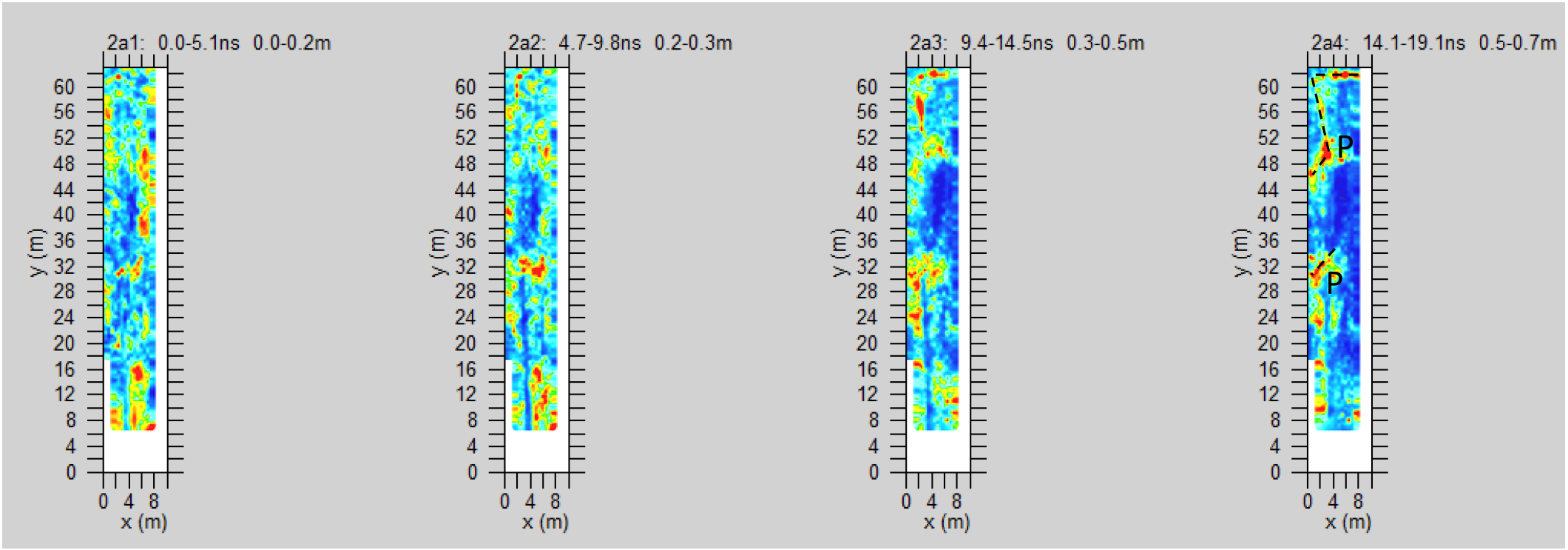

Fig. 10: Area B: depth slices 0-0.7m

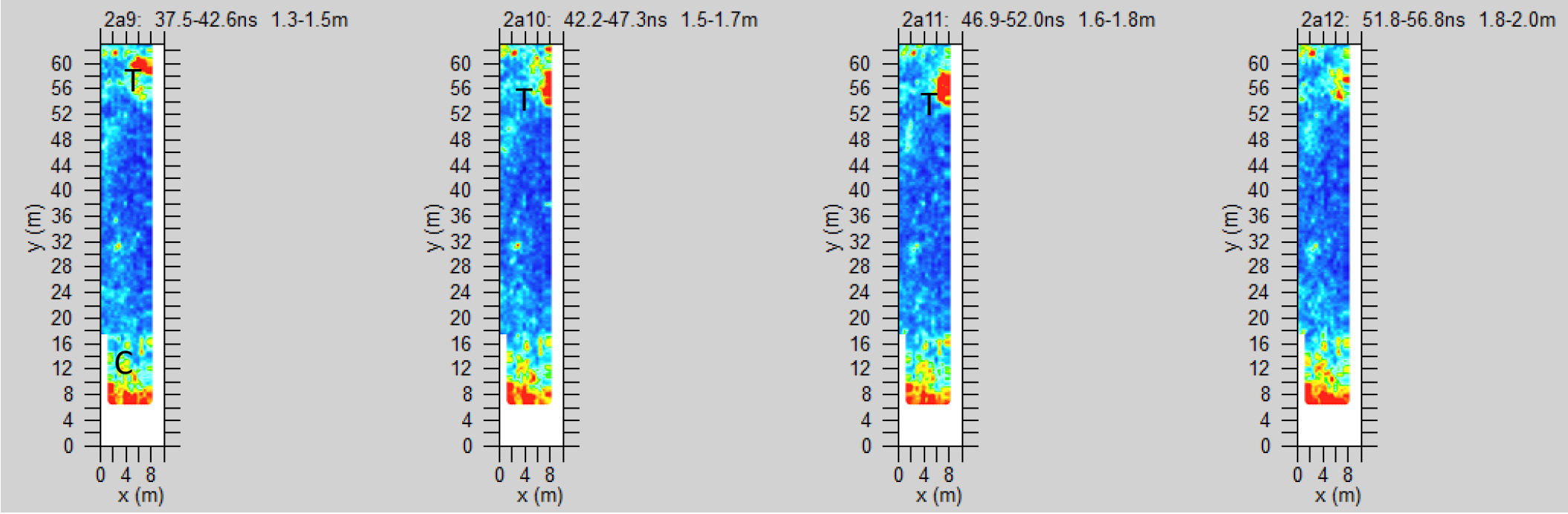

Fig. 11: Area B: depth slices 1.3-2.0m

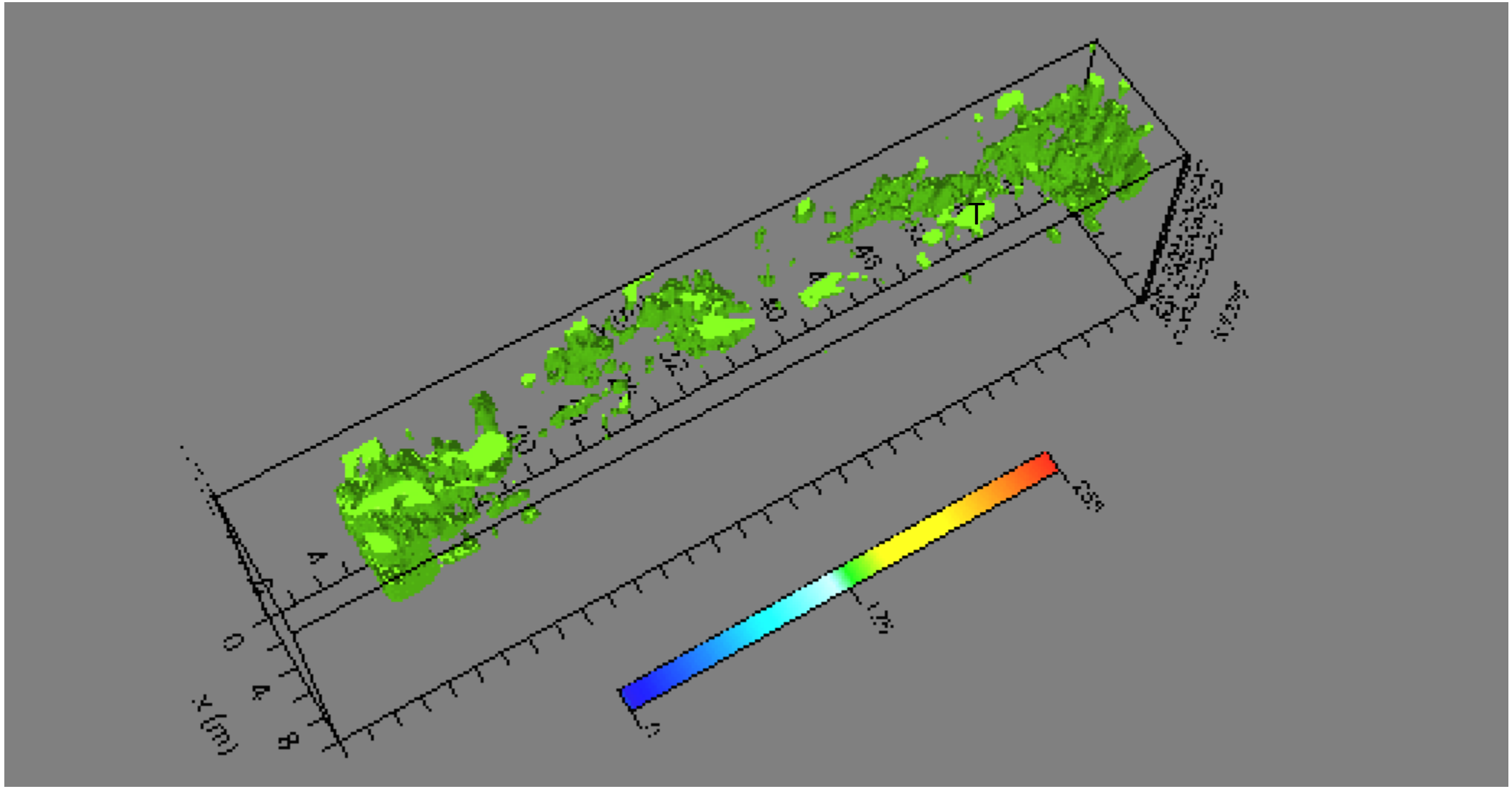

Fig. 12: Area B: iso-surfaces

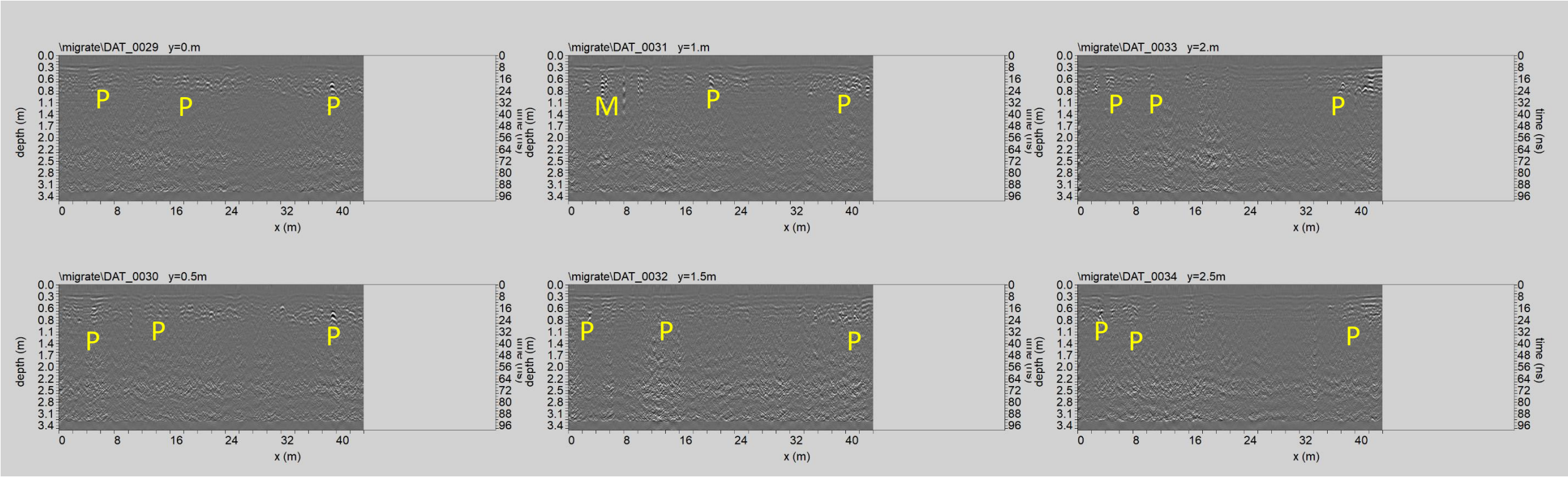

Fig. 13: Area C: GPR data processed related to the profiles 29, …, 34

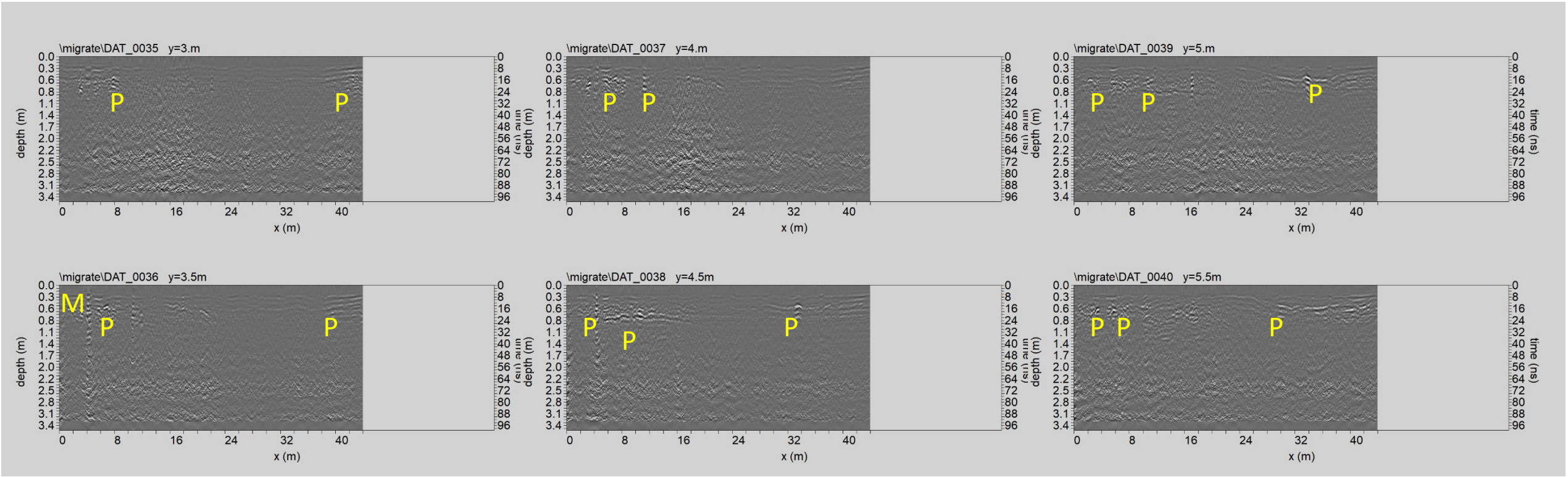

Fig. 14: Area C: GPR data processed related to the profiles 35, …, 40

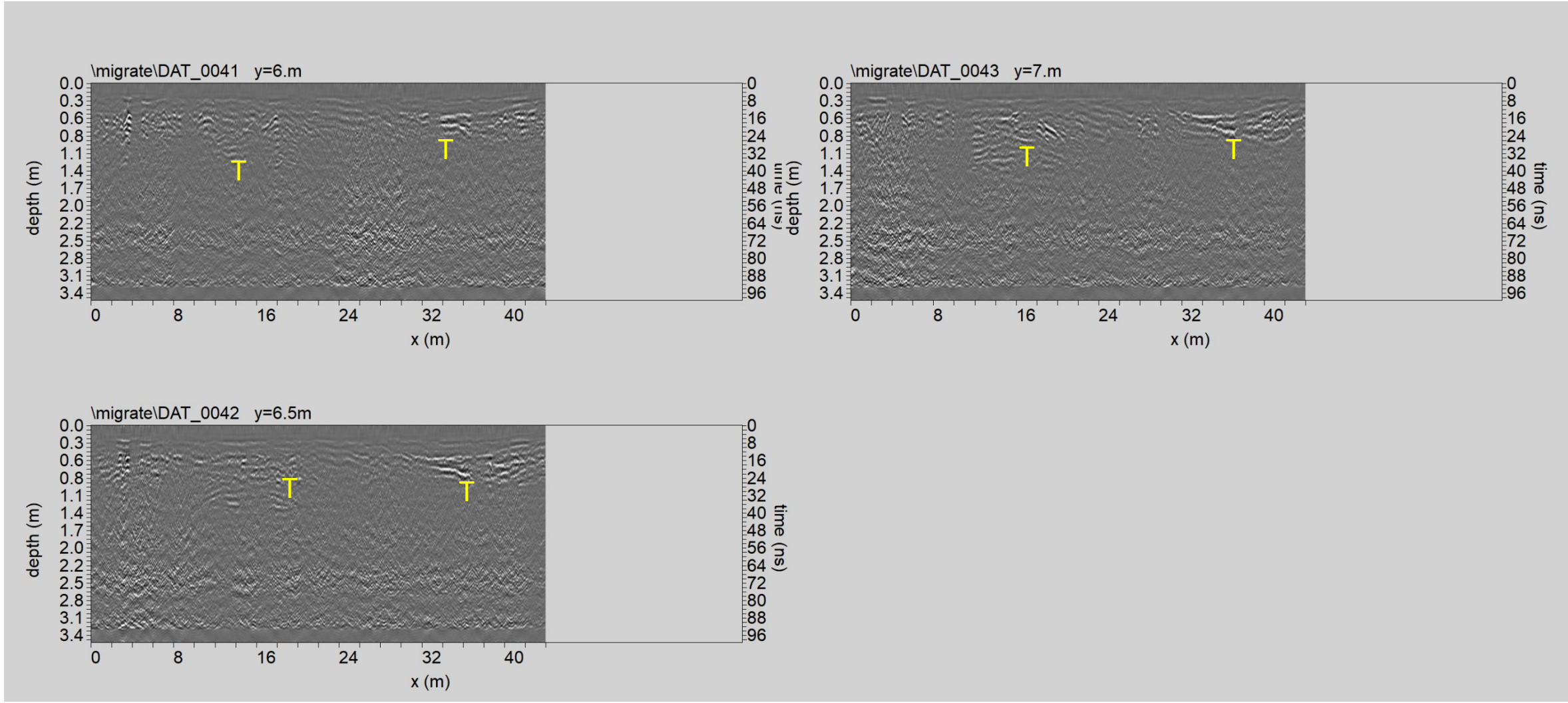

Fig. 15: Area C: GPR data processed related to the profiles 41, …, 43

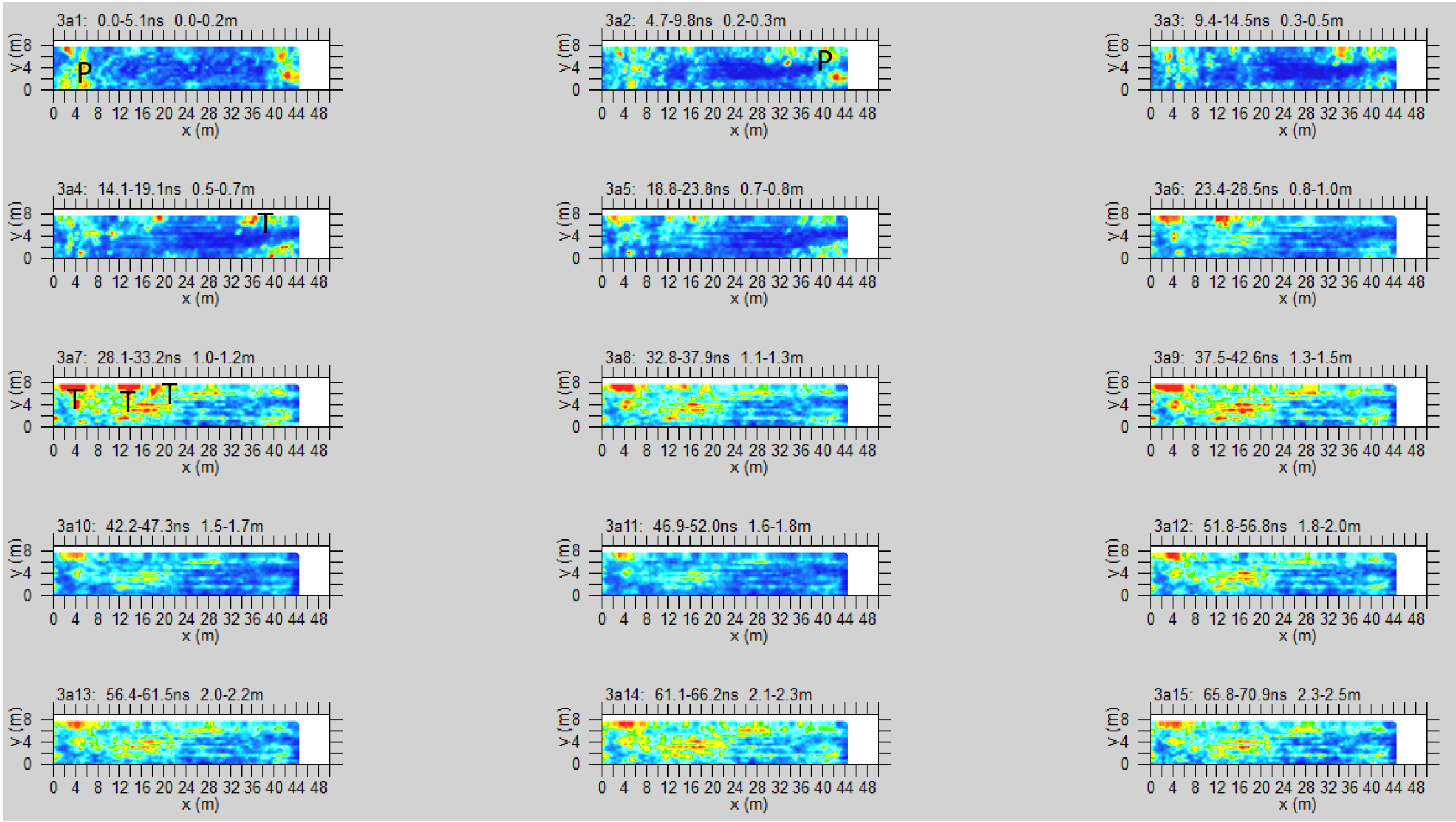

Fig. 16: Area C: depth slices

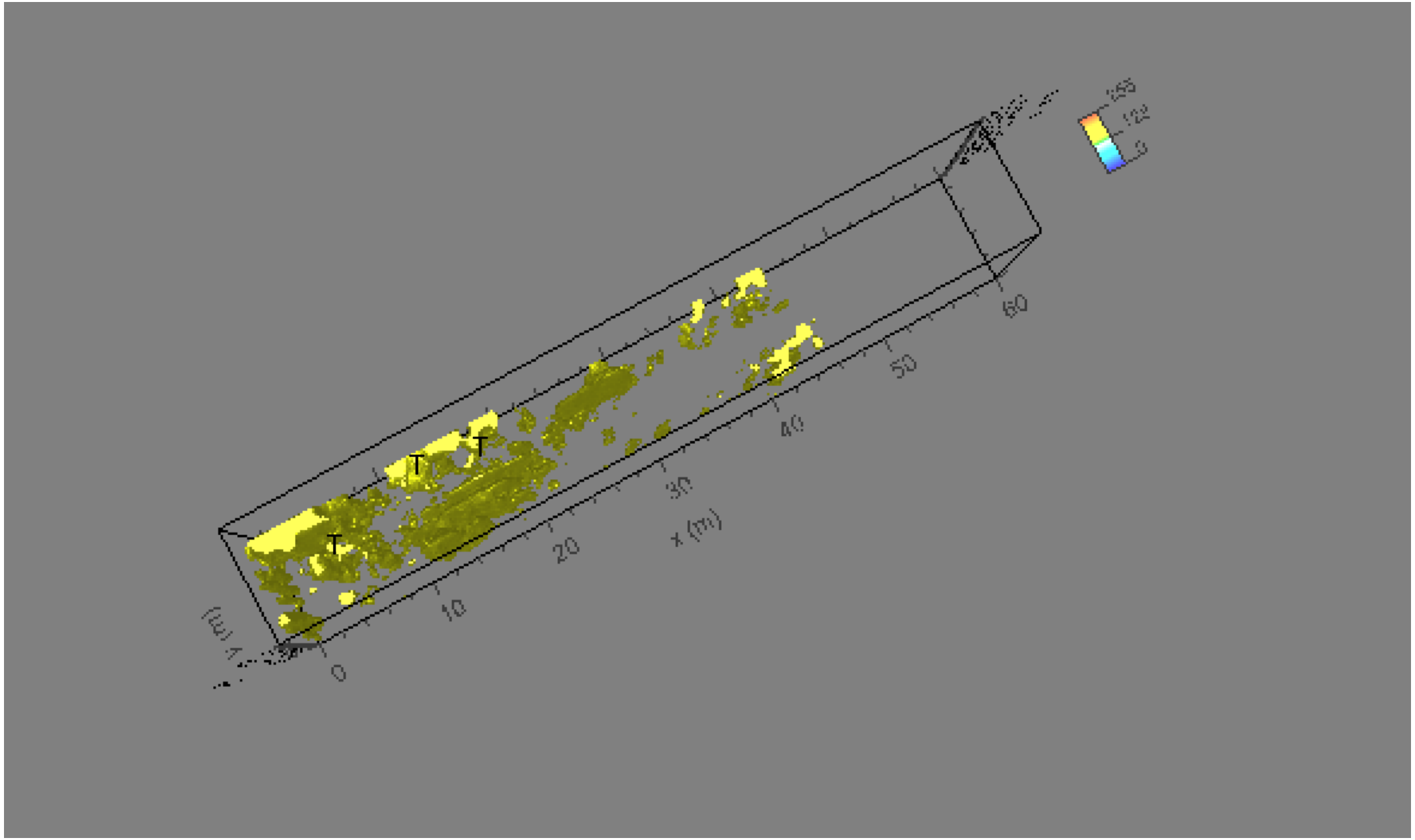

Fig. 17: Area C: iso-surfaces

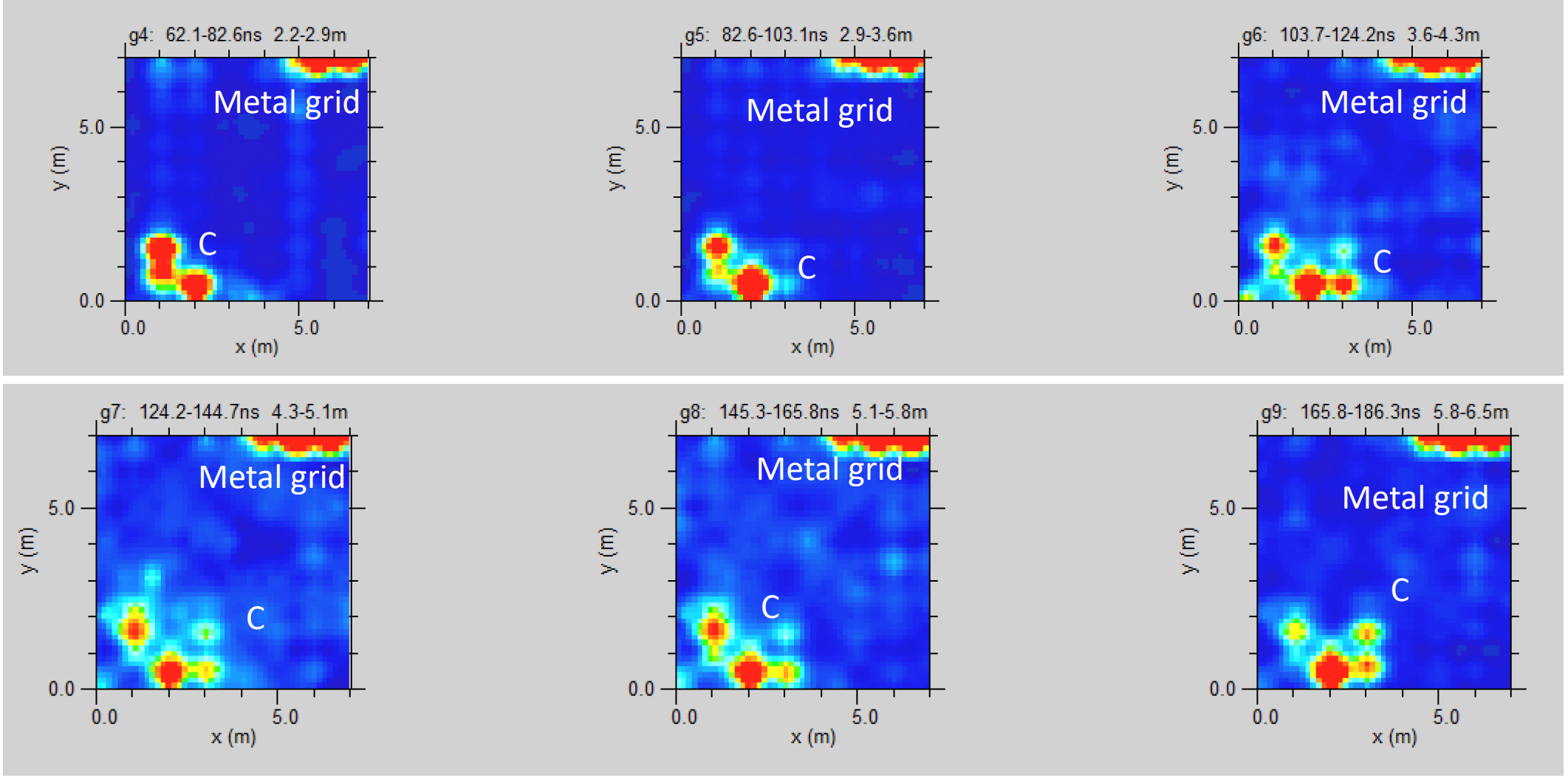

Fig. 18: Area E: depth slices

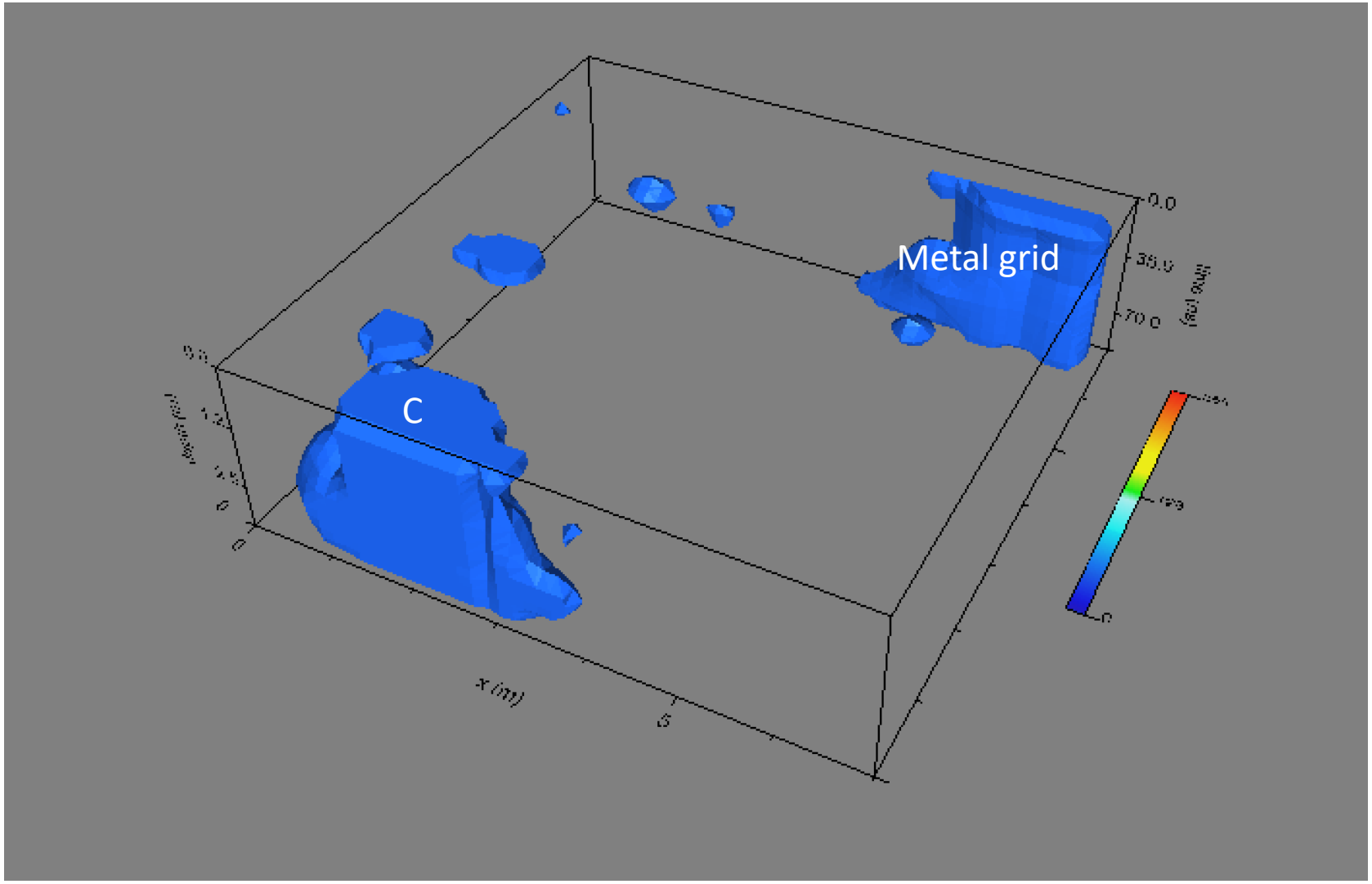

Fig. 19: Area E: iso-surfaces

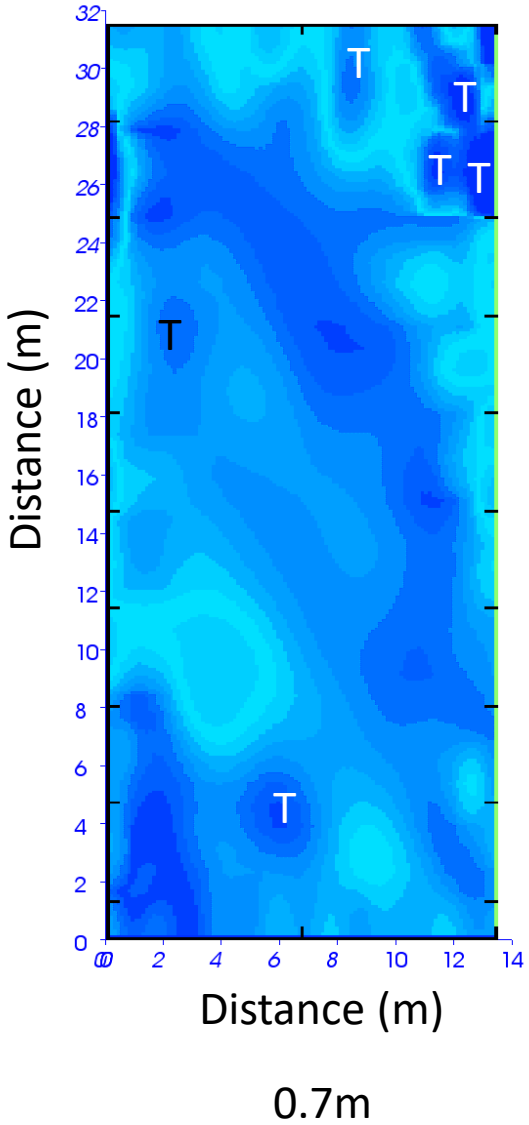

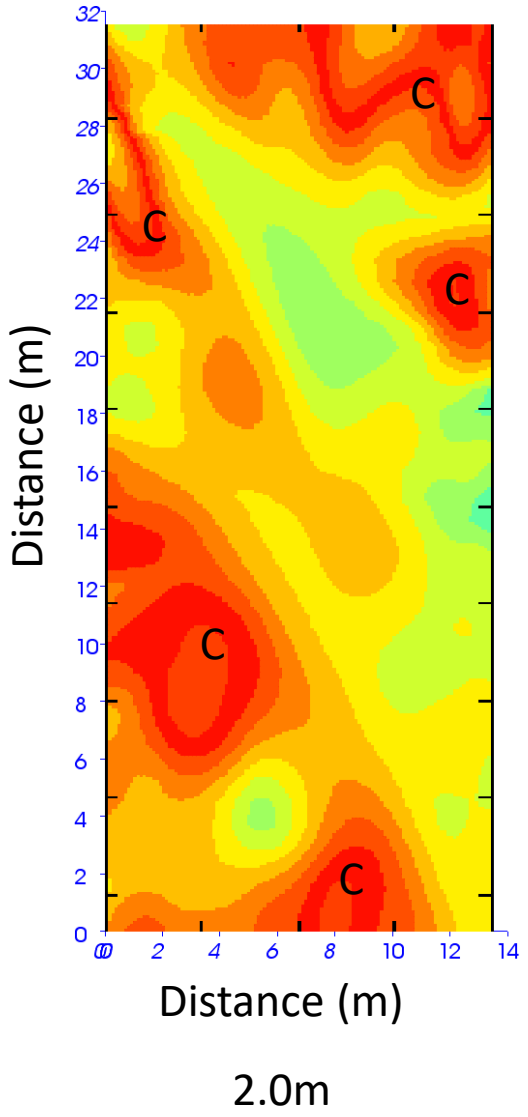

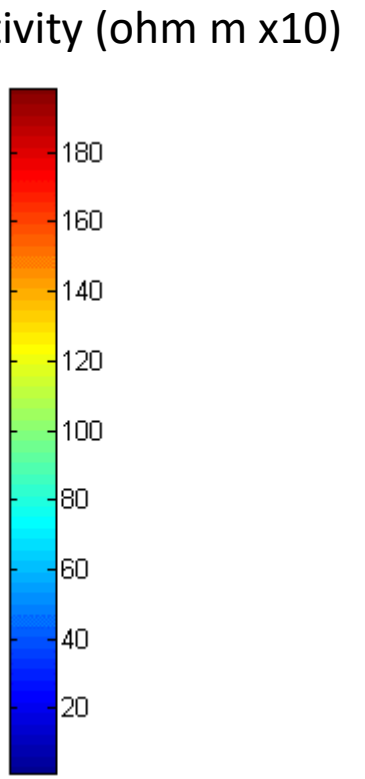

Fig. 20: Area D: ERT depth slices

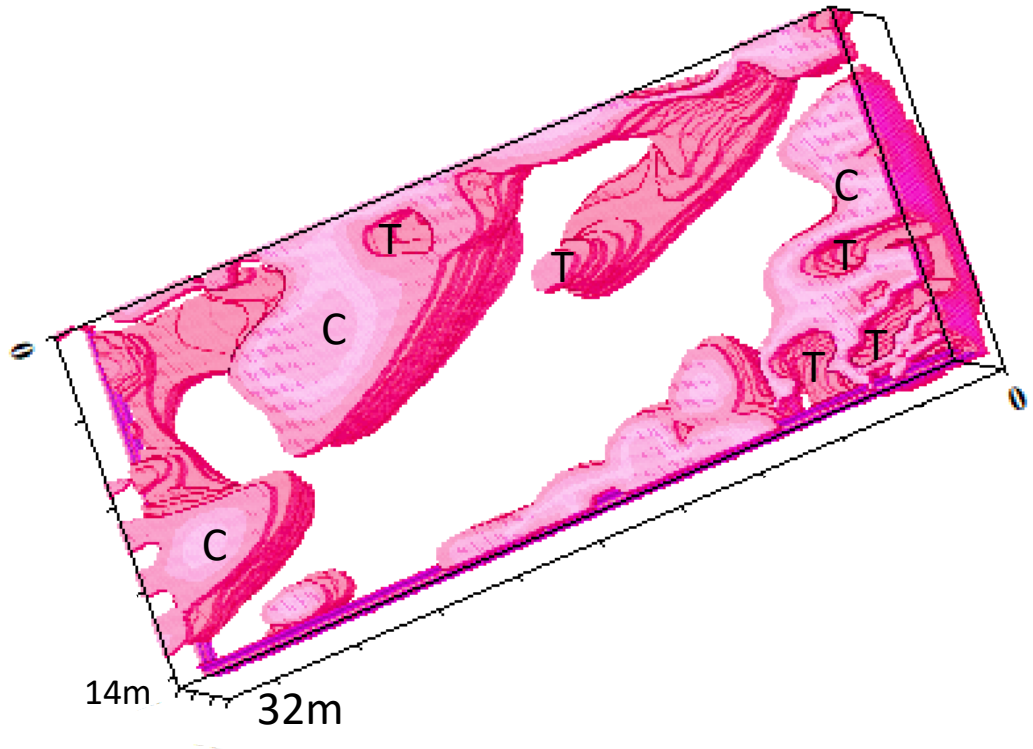

Fig. 21: Area D: resistivity iso-surfaces

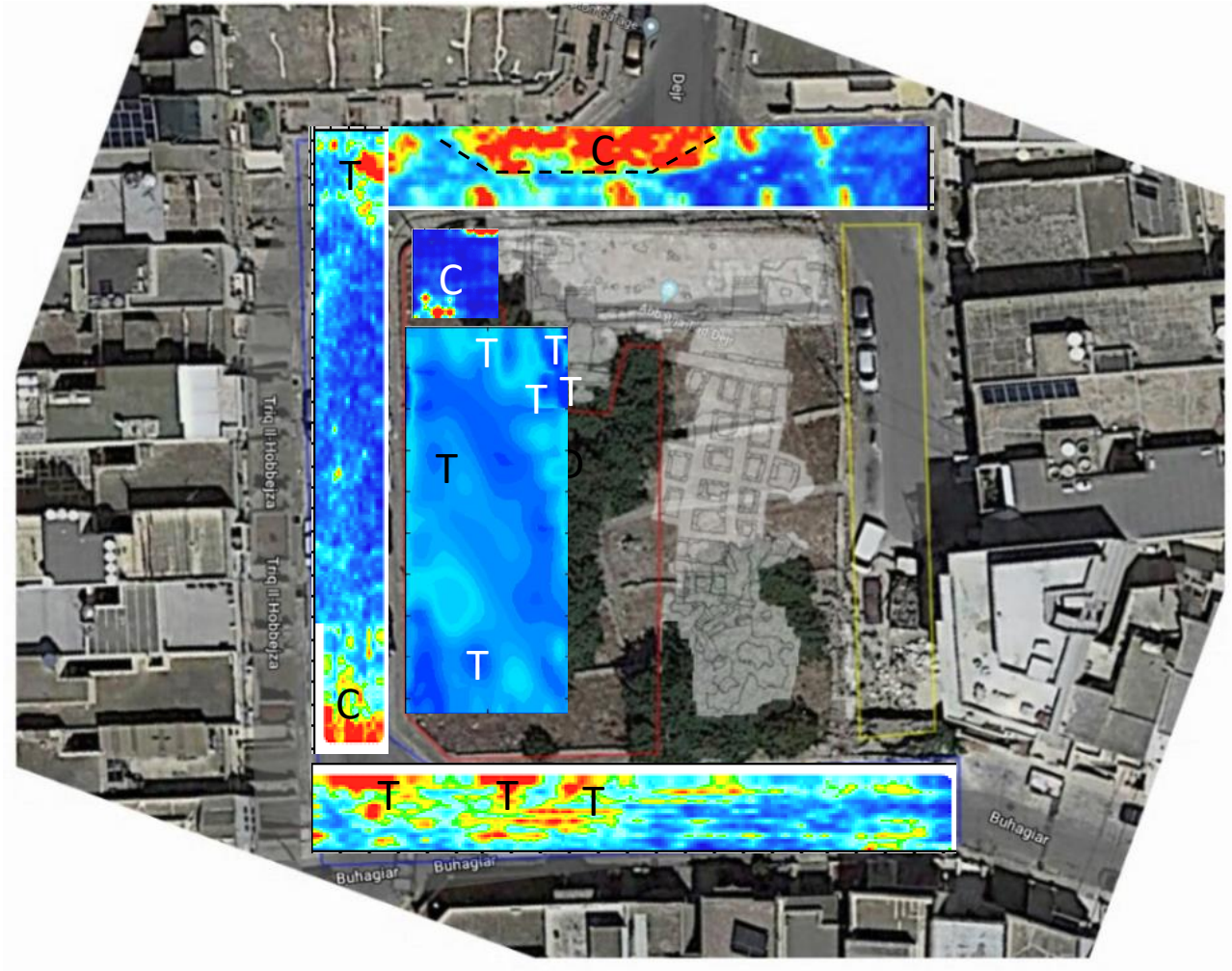

Fig. 21: slices overlapped the surveyed areas

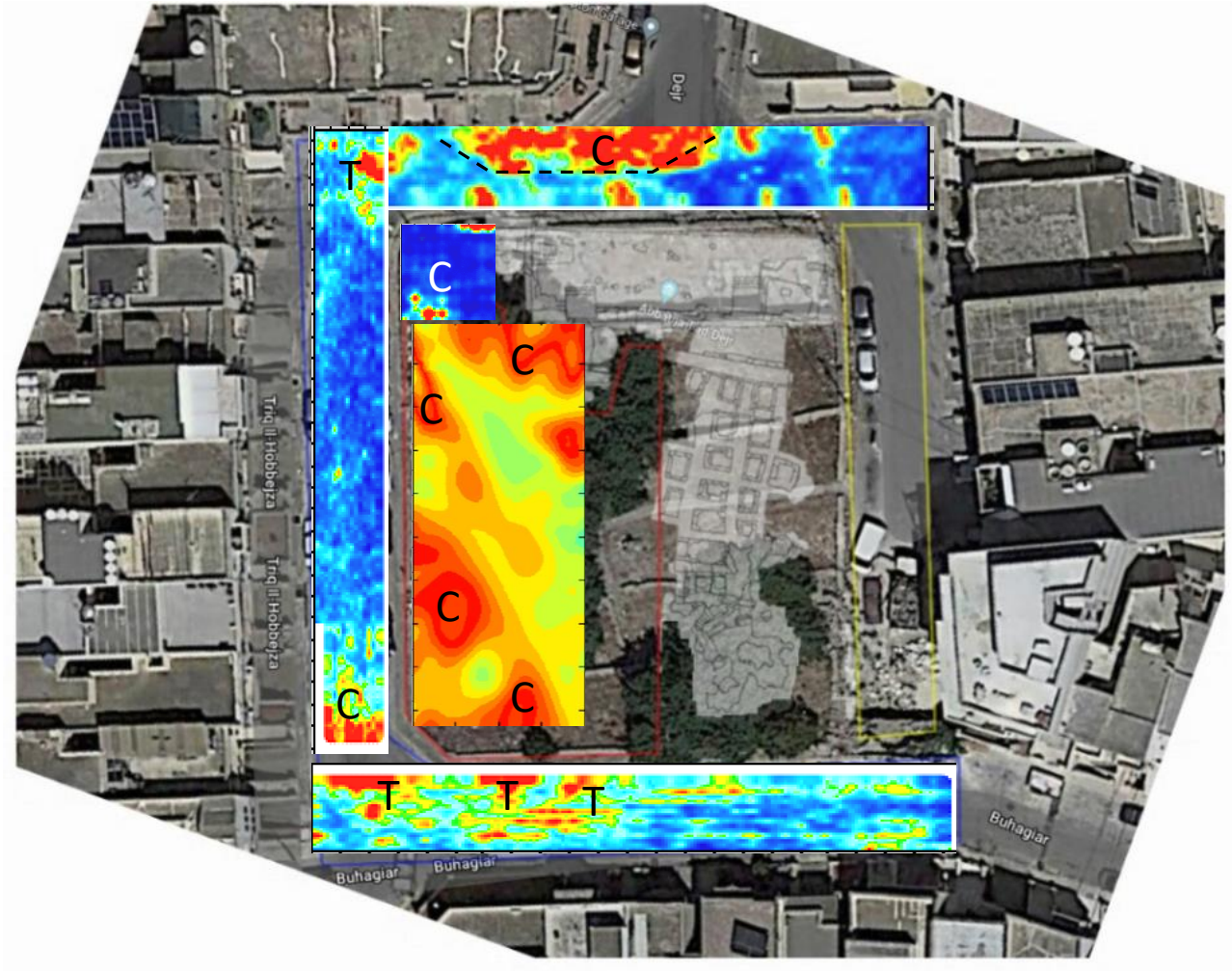

Fig. 22: slices overlapped the surveyed areas